JCI The Journal of Clinical Investigation

Group IIA secreted phospholipase A2 is associated with the pathobiology leading to COVID-19 mortality

Justin M. Snider, … , Maurizio Del Poeta, Floyd H. Chilton

J Clin Invest. 2021. https://doi.org/10.1172/JCI149236.

Research In-Press Preview **COVID-19** **Inflammation**

There is an urgent need to identify cellular/molecular mechanisms responsible for severe COVID-19 progressing to mortality. We initially performed untargeted/targeted lipidomics and focused biochemistry on 127 plasma samples and found elevated metabolites associated with secreted phospholipase A2 (sPLA2) activity and mitochondrial dysfunction in severe COVID-19 patients. Deceased COVID-19 patients had higher levels of circulating, catalytically active sPLA2 Group IIA (sPLA2-IIA), with a median value 9.6-fold higher than mild patients and 5.0-fold higher than severe COVID-19 survivors. Elevated sPLA2-IIA levels paralleled several indices of COVID-19 disease severity (e.g., kidney dysfunction, hypoxia, multiple organ dysfunction). A decision tree generated by machine learning identified sPLA2-IIA levels as a central node in stratifying patients that succumbed to COVID-19. Random forest analysis and LASSO-based regression analysis additionally identified sPLA2-IIA and blood urea nitrogen (BUN) as the key variables among 80 clinical indices in predicting COVID-19 mortality. The combined PLA-BUN index performed significantly better than either alone. An independent cohort (n=154) confirmed higher plasma sPLA2-IIA levels in deceased patients vs. severe or mild COVID-19, with the PLA-BUN index-based decision tree satisfactorily stratifying mild, severe, and deceased COVID-19 patients. With clinically tested inhibitors available, this study supports sPLA2-IIA as a therapeutic target to reduce COVID-19 mortality.

Find the latest version:

https://jci.me/149236/pdf

Group IIA Secreted Phospholipase A_2 is Associated with the Pathobiology Leading to COVID-19 Mortality

Justin M. Snider[1], Jeehyun Karen You[2], Xia Wang[3,4], Ashley J. Snider[1], Brian Hallmark[5], Manja M Zec[1], Michael C. Seeds[6], Susan Sergeant[7], Laurel Johnstone[8], Qiuming Wang[1], Ryan Sprissler[9,10], Tara F Carr[11], Karen Lutrick[12], Sairam Parthasarathy[13], Christian Bime[13], Hao Helen Zhang[14,15], Chiara Luberto[16,17], Richard R. Kew[17,18], Yusuf A. Hannun[17, 18, 19, 20, 21], Stefano Guerra[11], Charles E. McCall [22], Guang Yao[4,23], Maurizio Del Poeta[2, 21,24], Floyd H. Chilton[1,5*]

[1]Department of Nutritional Sciences, College of Agriculture and Life Sciences, University of Arizona, Tucson, AZ, USA
[2]Department of Microbiology and Immunology, Stony Brook University, Stony Brook, NY, USA
[3]School of Biomedical Engineering, Anhui Medical University, Hefei, PR China
[4]Department of Molecular and Cellular Biology, University of Arizona, Tucson, AZ, USA
[5]BIO5 Institute, University of Arizona, Tucson, AZ, USA
[6]Wake Forest Institute of Regenerative Medicine, Wake Forest School of Medicine Winston-Salem, NC, USA
[7]Department of Biochemistry, Wake Forest School of Medicine, Winston-Salem, NC, USA
[8]Research Innovation and Impact - Core Facilities, University of Arizona, Tucson, AZ, USA
[9]Center for Applied Genetics and Genomic Medicine, University of Arizona, Tucson, AZ, USA
[10]Department of Health Sciences, University of Arizona, Tucson, AZ, USA
[11]Asthma and Airway Disease Research Center, University of Arizona, Tucson, AZ, USA
[12]Family & Community Medicine, College of Medicine-Tucson, University of Arizona, Tucson, AZ, USA
[13]Division of Pulmonary, Allergy, Critical Care & Sleep Medicine, University of Arizona, Tucson, AZ, USA
[14]Department of Mathematics, University of Arizona, Tucson, AZ, USA
[15]Statistics Interdisciplinary Program, University of Arizona, Tucson, AZ, USA
[16]Department of Physiology and Biophysics, Stony Brook University, Stony Brook, NY, USA [14]
[17]Stony Brook Cancer Center, Stony Brook, NY, USA
[18]Department of Pathology, Stony Brook University, Stony Brook, NY, USA
[19]Department of Medicine, Stony Brook University, Stony Brook, NY, USA
[20]Department of Biochemistry and Cell Biology, Stony Brook University, Stony Brook, NY, USA
[21]Veteran Affairs Medical Center, Northport, NY, USA
[22]Departments of Internal Medicine, Microbiology and Immunology and Translational Sciences Institute, Wake Forest School of Medicine, Winston Salem, North Carolina, USA
[23]Arizona Cancer Center, University of Arizona, Tucson, AZ, USA
[24]Division of Infectious Diseases, Stony Brook University, Stony Brook, NY, USA

***Correspondence:** Floyd H. Chilton, PhD, BSRL Building, Room 370, 1230 N. Cherry Ave. Tucson, AZ 85719. email: fchilton@arizona.edu, phone: 520-621-5327

Conflict of Interest Statement: Maurizio Del Poeta is a co-founder and Chief Scientific Officer (CSO) of MicroRid Technologies Inc.

Abstract

There is an urgent need to identify cellular/molecular mechanisms responsible for severe COVID-19 progressing to mortality. We initially performed untargeted/targeted lipidomics and focused biochemistry on 127 plasma samples and found elevated metabolites associated with secreted phospholipase A_2 ($sPLA_2$) activity and mitochondrial dysfunction in severe COVID-19 patients. Deceased COVID-19 patients had higher levels of circulating, catalytically active $sPLA_2$ Group IIA (sPLA2-IIA), with a median value 9.6-fold higher than mild patients and 5.0-fold higher than severe COVID-19 survivors. Elevated $sPLA_2$-IIA levels paralleled several indices of COVID-19 disease severity (e.g., kidney dysfunction, hypoxia, multiple organ dysfunction). A decision tree generated by machine learning identified $sPLA_2$-IIA levels as a central node in stratifying patients that succumbed to COVID-19. Random forest analysis and LASSO-based regression analysis additionally identified $sPLA_2$-IIA and blood urea nitrogen (BUN) as the key variables among 80 clinical indices in predicting COVID-19 mortality. The combined PLA-BUN index performed significantly better than either alone. An independent cohort (n=154) confirmed higher plasma $sPLA_2$-IIA levels in deceased patients vs. severe or mild COVID-19, with the PLA-BUN index-based decision tree satisfactorily stratifying mild, severe, and deceased COVID-19 patients. With clinically tested inhibitors available, this study supports $sPLA_2$-IIA as a therapeutic target to reduce COVID-19 mortality.

Introduction

Host resistance and disease tolerance are paramount to mounting a successful defense against infections such as SARS-CoV-2. Up to 80% of individuals infected with SARS-CoV-2 are asymptomatic or develop mild to moderate symptoms. However, others progress to severe disease with life-threatening complications, requiring hospitalization and specialized medical care. Severe COVID-19 correlates with respiratory symptoms (i.e. dyspnea, hyperpnea, hypoxemia, pulmonary infiltration) and concomitant multiple organ failure with disseminated intravascular coagulation (1). Consequently, there is an urgent need to elucidate central molecular mechanisms that underly severe and fatal COVID-19 disease to develop targeted therapeutic approaches.

Early studies suggested that the host response to COVID-19 may be associated with an excessive proinflammatory response caused by a cytokine storm syndrome (CSS) (2). However, more recent studies show that persistent CSS is uncommon (3-4%) in severe COVID-19 disease, where high-dose steroids benefit only a small proportion of individuals with organ failure (3, 4). Mounting evidence supports that immunometabolic suppression and not CSS compromises host immunity, leading to unrestrained viral replication and severe COVID-19 (5, 6). Even when viral burdens decrease, pathologies including tissue and organ damage often remain (7).

Lipid metabolism plays an important role in determining COVID-19 outcomes. Early lipidomic studies (8, 9) revealed that severe COVID-19 modifies the circulating lipidome, with decreases in plasma levels of phospholipids and elevated quantities of lyso-phospholipids (lyso-PL), unesterified unsaturated fatty acids (UFA), and acylcarnitines. This lipidomic pattern suggests that severe COVID-19 may be accompanied by cellular or circulating phospholipase(s) that cleave intact phospholipids from cellular and mitochondrial membranes to form lyso-PL and UFA. Among phospholipases, the secreted phospholipase A_2 ($sPLA_2$) family includes 12 members with highly conserved characteristics, including low molecular weight (13-17 kDa), high Ca^{2+} levels for

catalytic activity, and the presence of histidine/aspartic acid dyads in the catalytic site (10). Elevated $sPLA_2$-IIA levels have been associated with various clinical conditions, including sepsis and systemic bacterial infections, adult respiratory disease syndrome (ARDS), atherosclerosis, cancer, and multiple organ trauma (10). Basal levels of circulating $sPLA_2$-IIA in healthy humans are 1-3 ng/ml; however, $sPLA_2$-IIA plasma concentrations can reach 250-500 ng/ml during acute sepsis (11).

Here, we identified lipidomic signatures of PLA_2 hydrolysis and mitochondrial dysfunction that correspond with COVID-19 severity in 127 patient plasma samples. Marked elevations in circulating $sPLA_2$-IIA levels mirrored disease severity, particularly in deceased COVID-19 patients. Circulating $sPLA_2$-IIA was catalytically active and paralleled several indices of disease severity, including hyperglycemia, kidney dysfunction, hypoxia, anemia, and multiple organ dysfunction. Importantly, three independent machine learning approaches identified $sPLA_2$-IIA as the central feature in predicting survivors from non-survivors in severe COVID-19 cases. Since blood urea nitrogen (BUN) was identified alongside plasma $sPLA_2$-IIA as a key stratification feature, we evaluated a novel PLA-BUN index as a prognostic biomarker of COVID-19 related mortality. Indeed, our PLA-BUN index successfully predicted COVID-19 mortality, significantly better than either feature alone. A validation cohort (n=154) recapitulated the increases in plasma $sPLA_2$-IIA in deceased COVID-19 patients, with the PLA-BUN index accurately stratifying the severe and deceased patients. Collectively, our study provides evidence to support a novel, targeted therapeutic approach using clinically available $sPLA_2$-IIA inhibitors to reduce COVID-19 mortality.

Results

An initial cohort of 127 patient plasma samples collected between May and July 2020 from Stony Brook University Medical Center (Stony Brook) was analyzed. Plasma sampling information is summarized in Table S1. Non-COVID-19 and mild COVID-19 patients had significantly shorter hospital stays compared to severe and deceased COVID-19 patients. Overall, COVID-19 patients' samples were collected at comparable timepoints during their hospital stay, whereas non-COVID-19 patients' samples were collected towards the latter end of inpatient stay. Demographics and baseline clinical characteristics of the patients are shown in Table 1. Age differed across groups, with deceased COVID-19 patients older on average (Figure S1). There were no significant trends in BMI or obesity. Prevalence of various co-morbidities was comparable across groups, except for higher prevalence of rheumatologic disease in non-COVID-19 patients. Severe and deceased COVID-19 patients presented with enhanced signs and symptoms of disease, such as: elevated NEWS2 score and 7-category ordinal scale score, pulmonary infiltration, and low oxygen saturation requiring oxygen therapy (Table S2, Figure S1). Furthermore, severe and deceased COVID-19 patients experienced more complications, with more cardiac arrests, acute kidney injury/renal failure, bacterial pneumonia, ARDS, and sepsis (Figure S1). Patients that developed severe COVID-19 received various therapies to treat hypoxemia, ARDS, superimposed/ventilator-associated bacterial pneumonia, hyper-inflammation, acute kidney injury/renal failure, and sepsis. A majority (70-80%) of severe and deceased COVID-19 patients received corticosteroid therapy, which has been shown to attenuate the expression of $sPLA_2$-IIA and induce the synthesis of proteins that inhibit $sPLA_2$-IIA activity (12-15). However, more patients received vasopressors in the deceased group, possibly due to uncontrolled septic shock eventually leading to multi-organ failure and cardiac arrest (Table S3).

Initial studies were designed to identify lipidomic changes linked to COVID-19 outcomes. Untargeted lipidomic analysis of the plasma samples revealed that the most significant changes

in the lipid profile occurred in deceased COVID-19 patients (Figure 1A), with 181 unique molecules identified. Further analysis of the 20 most significant molecules demonstrated enrichment in metabolites associated with acylcarnitine and phospholipid metabolism (Figure 1B). Specifically, several lyso-phosphatidylethanolamine (lyso-PE) molecular species typified by C16eLysoPE and unsaturated fatty acids such as linoleic (18:2) and oleic acids (18:1) were elevated in severe/deceased COVID-19 patients (Figure 1C). Targeted lipidomics confirmed the untargeted analysis, showing significant increases in major molecular species of lyso-PE and lyso-phosphatidylserine (lyso-PS) while demonstrating no changes in lyso-phosphatidylcholine (lyso-PC) (Figure S2). Hydrolysis of PE, PS, but not PC to form corresponding lyso-PLs together with mobilization of unsaturated fatty acids such as linoleic and oleic acid are hallmarks of catalysis by a secreted PLA_2 isoform (16). Given the critical role of $sPLA_2$-IIA in several related diseases, these data suggest that PLA_2 hydrolysis (Figure 1D) may contribute to COVID-19 disease severity and mortality (10).

Severe and deceased COVID-19 patients also showed elevations in short- and medium-chain acylcarnitines (acetyl and hexanoyl carnitines) as well as mitochondrial DNA (mtDNA) (Figure 1C, Figure S3B). Moreover, acetylcarnitine exhibited high areas under ROC curves: 0.810 (95% CI, 0.694-0.925) for mild vs. severe and 0.849 (95% CI, 0.752-0.945) for mild vs. deceased (Figure S3A). Accordingly, acetylcarnitine may also be an indicator of COVID-19 severity and mortality. Circulating short chain acylcarnitines (particularly acetylcarnitine) was recently reported as a prognostic biomarker of death during sepsis (17). Plasma concentrations of mitochondrially encoded cytochrome B (MT-CYB) and cytochrome c oxidase subunit III (MT-COX3) were also significantly elevated in deceased COVID-19 patients compared to non-COVID-19 and mild COVID-19 patients (Figure S3B). Increases in mtDNA levels confirm results from a report linking mtDNA levels to COVID-19 severity and mortality (18). Together, these data also implicate defective fatty acid oxidation and mitochondrial dysfunction in COVID-19 severity and mortality.

$sPLA_2$-IIA levels were subsequently quantified in the 127 plasma samples to corroborate our lipidomic analyses. Figure 2A shows the distribution of $sPLA_2$-IIA levels with markedly higher median values in deceased (89.3 ng/ml) and severe (17.9 ng/ml) COVID-19 patients compared to mild COVID-19 (9.3 ng/ml) and non-COVID-19 patients (8.9 ng/ml). Given non-COVID-19 patients in this cohort showed higher prevalence of rheumatologic disease compared to COVID-19 patients (Table 1, Figure S1), it is important to note that rheumatologic diseases significantly increase plasma $sPLA_2$-IIA levels (19) when compared to healthy control individuals (median = 0 ng/ml, interquartile range: 0–6.5) (20). Importantly, deceased COVID-19 patients had $sPLA_2$-IIA levels as high as 1,020 ng/ml and overall levels were 9.6 and 5.0-fold greater than mild and severe COVID-19 patients, respectively. Furthermore, circulating $sPLA_2$-IIA was catalytically active (Figure 2B), and its potential pathologic impact on organism-wide membranes was supported by a strong correlation ($r^2 = 0.84$, $p = 1.2 \times 10^{-13}$) between $sPLA_2$-IIA concentrations and enzymatic activity (Figure 2C).

Elevated levels of plasma $sPLA_2$-IIA were significantly associated with several clinical indices (Figure 2D). Positive correlations with higher baseline NEWS2 and 7-category ordinal scale scores suggest a role for $sPLA_2$-IIA in disease severity. The positive correlation of $sPLA_2$-IIA with glucose levels highlights a potential link to dysregulated systemic inflammation. Accordingly, hyperglycemia is an important prognostic factor for COVID-19 and associates with a pro-oxidative/proinflammatory state (21). The positive correlations with creatinine and BUN levels (and a corresponding negative correlation with glomerular filtration rate (GFR)) demonstrate how $sPLA_2$-IIA levels may also reflect kidney dysfunction. Finally, the negative correlations of $sPLA_2$ levels with hematocrit, hemoglobin levels, and oxygen saturation further support that $sPLA_2$-IIA may contribute to disease severity including hypoxemia and multiple organ dysfunction (22).

Three parallel unbiased machine learning analyses also identified elevated $sPLA_2$-IIA as a critical risk factor for COVID-19 mortality. First, eighty clinical indices including $sPLA_2$-IIA levels in the

initial cohort of 127 patients were analyzed in a clinical decision tree model (23). A decision tree generated by recursive partitioning identified critical indices necessary to stratify the four patient groups with high accuracy (area under ROC curve = 0.93-1.0, Figure 3A inset). Patients positive for COVID-19 were stratified using the predictor "7-category ordinal scale" into "mild" and "severe or deceased", with 91% and 100% accuracy, respectively. Surprisingly, $sPLA_2$-IIA level was identified as the central node that stratified survivors from non-survivors in the “severe or deceased” category. Indeed, no severe patients with $sPLA_2$-IIA levels of < 10 ng/mL died from COVID-19. In contrast, 75.4% of the patients in the “severe or deceased” category had $sPLA_2$-IIA levels ≥ 10 ng/mL, and 63% of this subset succumbed to the disease. Of the remaining patients with high $sPLA_2$-IIA levels (≥ 10 ng/mL), those with BUN levels < 16 mg/dL all survived. Conversely, 76% of the patients with high $sPLA_2$-IIA levels (≥ 10 ng/mL) and BUN levels ≥ 16 mg/dL succumbed to the disease. The clinical decision tree developed in this study provides a framework to identify COVID-19 patients at high risk for progressing to mortality. Out of eighty clinical indices measured, circulating levels of $sPLA_2$-IIA emerged as the most important prognostic factor for COVID-19-related mortality. A cutoff value of ≥ 10 ng/mL accurately predicted mortality in severe COVID-19 patients. Combining $sPLA_2$-IIA and BUN levels into a PLA-BUN index ($sPLA_2$-IIA ≥ 10 ng/mL and BUN ≥ 16 mg/dL) resulted in a parameter that predicted COVID-19 mortality more accurately than using either one alone (Figure 3B and 3C).

To separately assess and rank the relative importance of the eighty clinical indices (features) in predicting COVID-19 mortality, two additional machine learning approaches were used. A random forest analysis ranked feature importance by removing a feature from the model and then evaluating the corresponding decrease in prediction accuracy obtained from an assembly of decision trees (n = 1,000 each in 10 repeats, Figure 4A) (24). This method identified $sPLA_2$-IIA and BUN as the top 2 features, ranking significantly higher ($p < 0.0001$) than all other clinical indices (including age and BMI) in accurately predicting COVID-19 related mortality (Figure 4B

and C). A logistic regression model using LASSO also identified $sPLA_2$-IIA and BUN as two of the six features selected among the 80 clinical variables to classify severe and deceased patients (Supplementary Table 4) (25). Figure S4 illustrates that three independent machine learning approaches found $sPLA_2$-IIA and BUN to be key features for predicting COVID-19 mortality.

A second independent test cohort of mild, severe, or deceased patient plasma samples (n=154) were obtained from both Banner-University Medical Center Tucson (Banner) and Stony Brook. The clinical decision tree that minimized the classification error in the first cohort was applied to this cohort. Consistently, $sPLA_2$-IIA levels were significantly higher in deceased patients than in severe and mild (Figure S5A), with the PLA-BUN index-based decision tree model stratifying the patient groups (mild, severe, and deceased) with reasonably high accuracy (AUC = 0.72-0.99, Figure S5B; also see the decision surface plot, Figure S5C).

Given the potential for cross reactivity in antibody-based assays due to extensive homology across numerous $sPLA_2$ isoforms, ELISA results were validated using a proteomics assay with greater specificity. SomaScan (aptamer-based proteomics) analysis of the Banner samples validated the presence of the Group IIA $sPLA_2$ isoform in the plasma of COVID-19 patients in both severe and deceased COVID-19 patients compared to non-COVID-19 patients (Figure S6). SomaScan data are compositional and therefore not quantitative like the ELISA-based quantitation we utilized for both our initial and validation cohorts.

In a subset of sequential samples (n=46) for which each patient's plasma was sampled at two timepoints, $sPLA_2$-IIA levels tapered in the "late" compared to "early" samples in the mild and severe groups but remained relatively constant in deceased patients (median $sPLA_2$-IIA levels in linear scale dropped by 60.2%, 62.0%, and 18.7%, respectively, in mild, severe, and deceased) (Figure S7). Given the limited number of sequential samples available, the differences in $sPLA_2$-IIA level between timepoints were not statistically significant for mild or severe COVID-19 patients.

However, these trends are consistent with the possible role of $sPLA_2$-IIA in COVID-19 mortality. Moreover, these data suggest that monitoring $sPLA_2$-IIA levels in severe COVID-19 patients may be clinically useful.

Discussion

Early studies from the 1980s first described elevated circulating PLA_2 activity in severe sepsis, mirroring our observations in this study (26-28). Indeed, patients who succumbed to sepsis showed sustained and increasing trends in PLA_2 activity whereas survivors showed marked tapering. While it was not possible to determine the temporal nature of $sPLA_2$-IIA levels in these retrospective cohorts with a limited number of sequential samples, deceased COVID-19 patients had persistently elevated $sPLA_2$-IIA levels. When activated, $sPLA_2$-IIA has direct and organism-wide pathogenic potential (10, 29-32), which may contribute to COVID-19 severity and mortality (Figure 5). During cell activation and initiation of multiple cell death mechanisms, anionic phospholipids PS and PE are externalized, exposing them to phospholipid hydrolysis by $sPLA_2$-IIA (33). Hydrolysis of cellular membranes can broadly invoke tissue damage and organ dysfunction. Additionally, activated cells and damaged tissues/organs secrete extracellular mitochondria (29). Given mitochondrial phospholipids are preferred substrates for $sPLA_2$-IIA, our data suggest cell catalysis resulting in release of mtDNA, acetylcarnitine, and several danger-associated molecular patterns (DAMPs) (34) during severe COVID-19 disease. Damaged mitochondria can then be internalized by bystander leukocytes to increase inflammatory mediators including lyso-PLs, unsaturated fatty acids, eicosanoids, and cytokines. $sPLA_2$-IIA also hydrolyzes platelet-derived extracellular vesicles (EV) to release cyclooxygenase, thromboxane synthase, and 12-lipoxygenase inflammatory eicosanoids (10). Given the known properties of $sPLA_2$-IIA, our findings suggest that $sPLA_2$-IIA may prolong and exacerbate tissue and organ damage during fatal COVID-19 disease.

As a multi-institutional retrospective observational study, there are limitations. Since study patients were selected on plasma sample availability, the study is subject to potential confounders and may not represent the general population. Additionally, clinical data availability was restricted to existing medical records, and there were missing values in the dataset (especially in the second

cohort). Moreover, temporal relationships were difficult to assess as plasma sampling was not standardized. Given one of the test cohorts comprised plasma samples from two institutions, patient populations may be heterogeneous. Finally, given the chaotic nature of COVID-19 management in early 2020, current standards of care may differ. Despite these limitations, this study consistently identifies $sPLA_2$-IIA as a previously unrecognized and plausible life-threatening mechanism underlying COVID-19 severity and mortality. It also offers a clinical blueprint for identifying those COVID-19 patients at risk of death and supports $sPLA_2$-IIA as a potential therapeutic target. Our findings are further supported by the fact that high levels of $sPLA_2$ also predict clinical disease severity in children, both in the acute phase of COVID-19 and in those who develop multisystem inflammatory syndrome (35).

Considering the role of $sPLA_2$-IIA during other forms of critical illness that are often complicated by multiple organ failure and high mortality rates, structurally diverse classes of $sPLA_2$-IIA inhibitors have been developed (36-40). Although deemed safe for clinical use, clinical trials using a $sPLA_2$-IIA inhibitor only improved survival in sepsis patients when treatment was initiated within 18 hours of organ failure (39,40). Further examination of these studies' design revealed limitations: 1) patient selection criteria did not incorporate patient $sPLA_2$-IIA levels and 2) circulating $sPLA_2$-IIA levels were not reported in the studies. Therefore, inappropriate patient selection likely contributed to patient heterogeneity, resulting in negative findings. A recent study reported that, using a cutoff value of 25 ng/ml, $sPLA_2$-IIA is highly sensitive and specific in detecting sepsis (20). Given that deceased COVID-19 patients in this study had elevated $sPLA_2$-IIA levels ($\geqslant$10 ng/ml), we propose incorporating $sPLA_2$-IIA levels and the newly identified PLA-BUN index as prognostic clinical parameters. Our study further highlights the merit of exploring $sPLA_2$-IIA inhibitors to reduce COVID-19 related morality.

Methods

Study Design

The study was designed according to Strengthening the Reporting of Observational Studies in Epidemiology (STROBE) guidelines (41). COVID-19 was diagnosed using the RT-PCR and COVID-19 positive patients were classified into 3 groups: 1) mild = mild symptoms without pneumonia on imaging and discharged from inpatient care, 2) severe = respiratory tract or non-specific symptoms, pneumonia confirmed by chest imaging, oxygenation index below 94% on room air, and discharged from inpatient care, 3) deceased = expired during inpatient care. All plasma samples were collected during each patient's inpatient hospital stay, except for the late (2^{nd}) timepoints for mild COVID-19 patients (Figure S6). Only non-COVID-19 and mild COVID-19 patients with NEWS2 scores ≤3 were included in this study in order to exclude patients hospitalized for unrelated, possibly confounding major clinical presentations.

Statistics

Untargeted lipidomic data were transformed, normalized, and analyzed using MetaboAnalyst 4.0. The Benjamini–Hochberg procedure was used to control the false discovery rate (FDR), and the molecules with FDR $\leqslant$ 0.1 and absolute $\log_2$ fold change (FC) $\geqslant$ 1.5 were considered as significant and biologically relevant. Individual metabolites, $sPLA_2$ levels, $sPLA_2$ activity, and mtDNA levels were compared between groups with non-parametric Mann-Whitney Wilcoxon tests at an α-level of 0.05 with an additional Holm adjustment for multiple comparisons. Spearman correlations between $sPLA_2$ levels and clinical indices were computed in R. Receiver operating characteristic (ROC) curves, area under the curves (AUC), and confidence intervals were generated using the R packages ROCR and pROC.

Decision Tree, Random Forest Analyses and Logistic Regression Analysis (LASSO)

Eighty initial clinical indices were used as input variables to build a predictive model (i.e., decision tree) by recursive partitioning, using the Classification and Regression Trees (CART) algorithm (23) implemented in the R package RPART. The tree model identified a set of predictive features (branch conditions) that best classified the initial cohort of 127 patients into the 4 groups: non-COVID-19, mild, severe, and deceased COVID-19 patients. The tree split points were determined by the Gini index with the minimum leaf size = 10. A tenfold cross-validation method was used to tune the tree model and evaluate its prediction accuracy. To avoid overfitting, the tree was pruned back to the smallest size while minimizing the cross-validated error. The classification accuracy of the tree to determine each group membership (e.g., deceased vs. non-deceased) was assessed using the area under the ROC curve.

To further evaluate the relative feature importance in accurately separating severe and deceased COVID-19 patients, a random forest analysis was performed using the R package Random Forest (24). An assembly of 1,000 random decision trees was constructed in each forest, and 10 forests were constructed in replicate. The importance of a given feature (i.e., one of the 80 clinical indices) was assessed by the decrease of prediction accuracy when such a feature was omitted in the model, based on two measurement metrics: Gini importance or Mean Decrease Impurity (MDI), and permutation importance or Mean Decrease Accuracy (MDA).

A logistic regression model was built to classify severe and deceased COVID patients using the *glmnet* package in R (25). The same 80 initial clinical indices used to construct the decision tree were used as the input variables; 48 indices with < 10 missing values (across the 60 total of severe and deceased in the initial cohort of 127 patients) were further reserved to construct the LASSO model, with the missing values imputed using the imputeMissing function (42). The classification accuracy of the LASSO model was determined by 10-fold cross-validation.

Sample Processing and Lipidomic Analyses

Frozen EDTA plasma samples were processed utilizing Biosafety Level 2 conditions as per CDC Guidelines for the handling and processing of specimens associated with Corona Virus Disease 2019. Metabolites were isolated from plasma via methanol-based containing 10 µl Splash Lipidomix (Avanti Polar Lipids, Alabaster, AL) and separated utilizing a reverse phase chromatography as previously described by Najdekr et al. (43). Samples were analyzed utilizing an UHPLC-ESI-MS/MS system (UHPLC, Thermo Horizon Vanquish Duo System, MS, Thermo Exploris 480) and separation was achieved utilizing an Hypersil GOLD aQ UPLC column (100 x 2.1 mm, 1.9 µm, Thermo Fisher Scientific, Part No. 25302-102130) with mobile phases composed of water containing 0.1% formic acid and methanol containing 0.1% formic acid. Metabolites were eluted over a 15 min gradient with the Exploris 480 operating in positive ion mode, utilizing an ion transfer tube temperature of 350 °C, sheath gas of 45, aux gas of 5, and spray voltage of 4000. MS data for all samples were collected using dynamic exclusion and then aligned with pooled samples collected using Thermo AquireX to achieve optimal metabolite identification in Lipid Search 4.0 and Thermo Compound Discoverer 2.3 software.

Targeted lipidomic analysis was performed using an Agilent 1200 HPLC tandem Thermo Quantum Ultra triple quadrupole mass spectrometer (Thermo Fisher Scientific, San Jose, USA) to quantify levels of major molecular species of lyso-phospholipids (lyso-PLs). C16, C18:1, C18:2, and C20:4 molecular species for lyso-phosphatidylcholine (lyso-PC), lyso-phosphatidylethanolamine (lyso-PE), and lyso-phosphatidylserine (lyso-PS) (Cayman Chemical, Ann Arbor, MI) were used as standards and deuterated Splash Lipidomix as internal standards. Lyso-PLs were separated using an Agilent Poroshell 120 EC-C18 1.9 µm (2.1x50 mm) with mobile phases composed of water containing 2 mM ammonium formate/0.1% formic acid (A) and methanol containing 1 mM ammonium formate/0.1% formic acid. Chromatographic gradient elution began at 40% A and remained there for the first minute, proceeding to 1% A at 6 minutes,

staying there for 10.5 min before returning to 40% MPA over 1.5 min and remaining till the end of the 20 min run.

Determination of $sPLA_2$-IIA Concentrations

$sPLA_2$-IIA levels in plasma were determined by ELISA (Cayman Chemical Company). Plasma samples were diluted (1:20-1:800) and assayed in duplicate. Concentrations of $sPLA_2$-IIA in plasma were calculated using standard curves.

Proteomic Analysis

Plasma samples from 82 Banner patients (21 non-COVID-19, 30 severe COVID-19 and 31 deceased COVID-19) were analyzed utilizing multiplexed SOMAscan and Selex processing technology by SomiLogic (Boulder, Colorado, USA). The aptamer based SomaScan assay (44) and its performance characteristics (45, 46), have previously been described and were utilized for the targeted analysis of nearly 7000 proteins, one of which was $sPLA_2$-IIA.

Enzymatic Assay for $sPLA_2$-IIA Activity

A subset of 34 patient samples from the initial Stony Brook cohort (n=127) was selected for PLA_2 activity analysis. sPLA2 activity was assayed by modifying techniques from Kramer and Pepinsky (47). Hydrolytic activity was determined in plasma samples from 34 patients (9 non-COVID-19, 8 mild, 7 severe, and 10 deceased COVID-19 patients) representing a wide range of $sPLA_2$-IIA levels. Assays contained 5 µl of plasma in a final volume of 400 µl containing 50 mM Tris/NaCl, pH 8.5, with 5 mM $CaCl_2$ and 5 nmol of 3H-oleate-labeled *E. coli* phospholipids and incubated for 30 mins at 37 °C. Lipids were extracted utilizing a modified Bligh and Dyer (48), and hydrolyzed fatty acids were separated from phospholipids using thin layer chromatography (Silica Gel G) and a mobile phase of hexane:ether:formic acid (90:60:6, v:v:v), and visualized by iodine vapor relative to cold standards.

Mitochondrial DNA Quantification

Mitochondrial DNA (mtDNA) was quantified in the same 34 patient samples as the enzymatic assay. Mitochondrial DNA (mtDNA) was quantified by adapting methods from Scozzi et al. (18). Using genes for human cytochrome C (MT-CYB) and cytochrome C oxidase subunit III (MT-COX3), mtDNA was quantified in plasma samples from the same 34 patients (9 non-COVID-19, 8 mild, 7 severe, and 10 deceased COVID-19 patients) as in the sPLA2 activity assay utilizing an ABI 7900HT real-time PCR instrument in 384-well format. Synthetic oligonucleotide copies of the MT-CYB and MT-COX3 genomic sequences (gBlock Gene Fragments from Integrated DNA Technologies) were included to generate a standard curve at 10^5, 10^4, 10^3, and 10^2 copies per µL. Primer sequences were as follows:

forward MT-CYB: 5'– ATGACCCCAATACGCAAAA-3'

reverse MT-CYB: 5'–CGAAGTTTCATCATGCGGAG-3'

forward MT-COX3: 5'–ATGACCCACCAATCACATGC-3'

reverse MT-COX3: 5'–ATCACATGGCTAGGCCGGAG-3'.

Each diluted serum sample was compared to a control reaction of a gBlock standard, and the delta-Ct was used to correct the calculated concentrations from triplicate reactions.

Study Approval

This retrospective study initially analyzed 127 plasma samples from patients hospitalized at Stony Brook (Stony Brook, NY, United States) from January to July 2020. This study was approved by the central IRB at Stony Brook University (IRB2020-00423). For the second independent cohort, the following 154 plasma samples were analyzed: Stony Brook (n=98) and Banner (n=56) hospitalized from January to November 2020. The Banner study was approved by the University of Arizona Human Subjects Protection Program (IRB2007847180).

Author Contributions

FHC conceived and designed the study. JKY, RRK, MDP, JMS, AJS, YAH and SS prepared IRB documentation, coordinated the collection of samples, and handled logistics of samples transfer between Stony Brook University Medical Center and the University of Arizona. KL, SP, CB and SG prepared IRB documentation, coordinated the collection of samples, and handled logistics of samples transfer between Banner-University Medical Center Tucson and the University of Arizona. JKY, SG, and MDP collected the clinical data. JMS, AJS and QW performed untargeted and targeted metabolomics and data analysis. MCS and SS performed $sPLA_2$ activity assay. AJS, MMZ, and TFC performed $sPLA_2$ ELISA. RS performed mitochondrial DNA analysis. XW, GY, BH, LJ and QW and HHZ did the statistical analysis and modeling. FHC and JMS wrote the initial manuscript draft. CEM, XW, JKY, MDP, YAH, AJS, CL, BH, and GY contributed to revisions and discussion.

Acknowledgements

The authors thank the Stony Brook Medicine Biobank for procuring and distribution of plasma samples from COVID-19 and non-COVID hospitalized patients. We acknowledge the University of Arizona Data Science Institute for their help in applying machine learning modeling.

References

1. Liao D, et al. Haematological characteristics and risk factors in the classification and prognosis evaluation of COVID-19: a retrospective cohort study. *Lancet Haematol.* 2020;7(9):e671-e678.
2. Fajgenbaum DC, June CH. Cytokine Storm. *N Engl J Med.* 2020;383(23):2255-2273.
3. Sinha P, et al. Is a "cytokine storm" relevant to COVID-19? *JAMA Intern Med.* 2020;180(9):1152-1154.
4. Horby P, et al. Dexamethasone in hospitalized patients with Covid-19 - Preliminary Report. *N Engl J Med.* 2020.
5. Remy KE, et al. Severe immunosuppression and not a cytokine storm characterizes COVID-19 infections. *JCI Insight.* 2020;5(17).
6. Zheng HY, et al. Elevated exhaustion levels and reduced functional diversity of T cells in peripheral blood may predict severe progression in COVID-19 patients. *Cell Mol Immunol.* 2020;17(5):541-543.
7. Nienhold R, et al. Two distinct immunopathological profiles in autopsy lungs of COVID-19. *Nat Commun.* 2020;11(1):5086.
8. Shen B, et al. Proteomic and metabolomic characterization of COVID-19 patient sera. *Cell.* 2020;182(1):59-72.e15.
9. Wu D, et al. Plasma metabolomic and lipidomic alterations associated with COVID-19. *Natl Sci Rev.* 2020;7(7):1157-1168.
10. Dore E, Boilard E. Roles of secreted phospholipase A(2) group IIA in inflammation and host defense. *Biochim Biophys Acta Mol Cell Biol Lipids.* 2019;1864(6):789-802.
11. van Hensbergen VP, et al. Type IIA secreted phospholipase A2 in host defense against bacterial infections. *Trends Immunol.* 2020;41(4):313-326.

12. Nakano, T, et al., Glucocorticoids suppress group II phospholipase A2 production by blocking mRNA synthesis and post-transcriptional expression*. J Biol Chem*. 1990;265(21):12745-8.

13 Miele, L. New weapons against inflammation: dual inhibitors of phospholipase A2 and transglutaminase*. J Clin Invest*. 2003;111(1): p. 19-21.

14. Kol S, et al. Glucocorticoids suppress basal (but not interleukin-1-supported) ovarian phospholipase A2 activity: evidence for glucocorticoid receptor-mediated regulation. *Mol Cell Endocrinol.* 1998;137(2):117-25.

15. Kuzniatsova O. Dexamethasone inhibits secretory and cytosolic phospholipases A2 in alveolar macrophages in acute lung injury. *Eur Respir J.* 2013;42(Suppl 57):P3863.

16. Dennis EA, et al. Phospholipase A2 enzymes: physical structure, biological function, disease implication, chemical inhibition, and therapeutic intervention. *Chem Rev.* 2011;111(10):6130-85.

17 Chung KP, et al. Increased plasma acetylcarnitine in sepsis is associated with multiple organ dysfunction and mortality: a multicenter cohort study. *Crit Care Med.* 2019;47(2):210-218.

18. Scozzi D, et al. Circulating mitochondrial DNA is an early indicator of severe illness and mortality from COVID-19. *JCI Insight.* 2021.

19. Boilard E, et al. A novel anti-inflammatory role for secretory phospholipase A2 in immune complex-mediated arthritis. *EMBO Mol Med.* 2010;2(5):172-187.

20. Berg E, et al. Measurement of a novel biomarker, secretory phospholipase A2 group IIA as a marker of sepsis: A Pilot Study. *J Emerg Trauma Shock.* 2018;11:135.

21. Ceriello A. Hyperglycemia and the worse prognosis of COVID-19. Why a fast blood glucose control should be mandatory. *Diabetes Res Clin Pract.* 2020;163:108186.

22. Hariyanto TI, Kurniawan A. Anemia is associated with severe coronavirus disease 2019 (COVID-19) infection. *Transfus Apher Sci.* 2020;59(6):102926.

23. Breiman L, et al. *Classification and Regression Trees.* Chapman & Hall; 1984.

24. Breiman L. Random Forests. *Mach Learn.* 2001;45(1):5-32.

25. Friedman J, et al. Regularization Paths for Generalized Linear Models via Coordinate Descent. *J Stat Softw.* 2010;33(1):1-22.

26. Vadas P. Elevated plasma phospholipase A2 levels: correlation with the hemodynamic and pulmonary changes in gram-negative septic shock. *J Lab Clin Med.* 1984;104(6):873-881.

27. Guidet B, et al. Secretory non-pancreatic phopholipase A2 in severe sepsis: relation to endotoxin, cytokines and thromboxane B2. *Infection.* 1996;24(2):103-108.

28. Vadas P, et al. A predictive model for the clearance of soluble phospholipase A2 during septic shock. *J Lab Clin Med.* 1991;118(5):471-475.

29. Boudreau LH, et al. Platelets release mitochondria serving as substrate for bactericidal group IIA-secreted phospholipase A2 to promote inflammation. *Blood.* 2014;124(14):2173-2183.

30. Hurt-Camejo E, et al. Phospholipase A(2) in vascular disease. *Circ Res.* 2001;89(4):298-304.

31. Chilton, F. Would the real role(s) for secretory PLA2s please stand up. *J Clin Invest.* 1996;97(10):2161-2.

32. Murakami M, et al. Regulatory Functions of Phospholipase A2. *Crit Rev Immunol.* 2017;37(2-6):127-95.

33. Atsumi G, et al. The perturbed membrane of cells undergoing apoptosis is susceptible to type II secretory phospholipase A2 to liberate arachidonic acid. *Biochim Biophys Acta.* 1997;1349(1):43-54.

34. Roh JS, Sohn DH. Damage-associated molecular patterns in inflammatory diseases. *Immune Netw.* 2018;18(4):e27.

35. Kuypers FA, et al. Secretory phospholipase A2 in SARS-CoV-2 infection and multisystem inflammatory syndrome in children (MIS-C). *Exp Biol Med (Maywood).* 2021:15353702211028560.

36. Tan TL, Goh YY. The role of group IIA secretory phospholipase A2 (sPLA2-IIA) as a biomarker for the diagnosis of sepsis and bacterial infection in adults-A systematic review. *PLoS One.* 2017;12(7):e0180554.

37. Anderson BO, et al. Phospholipase A2 regulates critical inflammatory mediators of multiple organ failure. *J Surg Res.* 1994;56(2):199-205.

38. Corke C, et al. Circulating secretory phospholipase A2 in critical illness--the importance of the intestine. *Crit Care Resusc.* 2001;3(4):244-249.

39. Zeiher BG, et al. LY315920NA/S-5920, a selective inhibitor of group IIA secretory phospholipase A2, fails to improve clinical outcome for patients with severe sepsis. *Crit Care Med.* 2005;33(8):1741-1748.

40. Abraham E, et al. Efficacy and safety of LY315920Na/S-5920, a selective inhibitor of 14-kDa group IIA secretory phospholipase A2, in patients with suspected sepsis and organ failure. *Crit Care Med.* 2003;31(3):718-728.

41. von Elm E, et al. The Strengthening the Reporting of Observational Studies in Epidemiology (STROBE) statement: guidelines for reporting observational studies. *Ann Intern Med.* 2007;147(8):573-7.

42. Meire M, et al. imputeMissings: Impute missing values in a predictive context. R package version 0.0.3. The Comprehensive R Archive Network. https://CRAN.R-project.org/package=imputeMissings. September 9, 2016. Accessed July 21, 2001.

43. Najdekr L, et al. Collection of Untargeted Metabolomic Data for Mammalian Urine Applying HILIC and Reversed Phase Ultra Performance Liquid Chromatography Methods Coupled to a Q Exactive Mass Spectrometer. *Methods Mol Biol.* 2019;1996:1-15.

44. Gold L, et al. Aptamer-based multiplexed proteomic technology for biomarker discovery. *PLoS One.* 2010;5(12):e15004.

45. Kim CH, et al. Stability and reproducibility of proteomic profiles measured with an aptamer-based platform. *Sci Rep.* 2018;8(1):8382.

46. Candia J, et al. Assessment of Variability in the SOMAscan Assay. *Sci Rep.* 2017;7(1):14248.

47. Kramer RM, Pepinsky RB. Assay and purification of phospholipase A2 from human synovial fluid in rheumatoid arthritis. *Methods Enzymol.* 1991;197:373-81.

48. Bligh EG, Dyer WJ. A rapid method of total lipid extraction and purification. *Can J Biochem Physiol.* 1959;37(8):911-7.

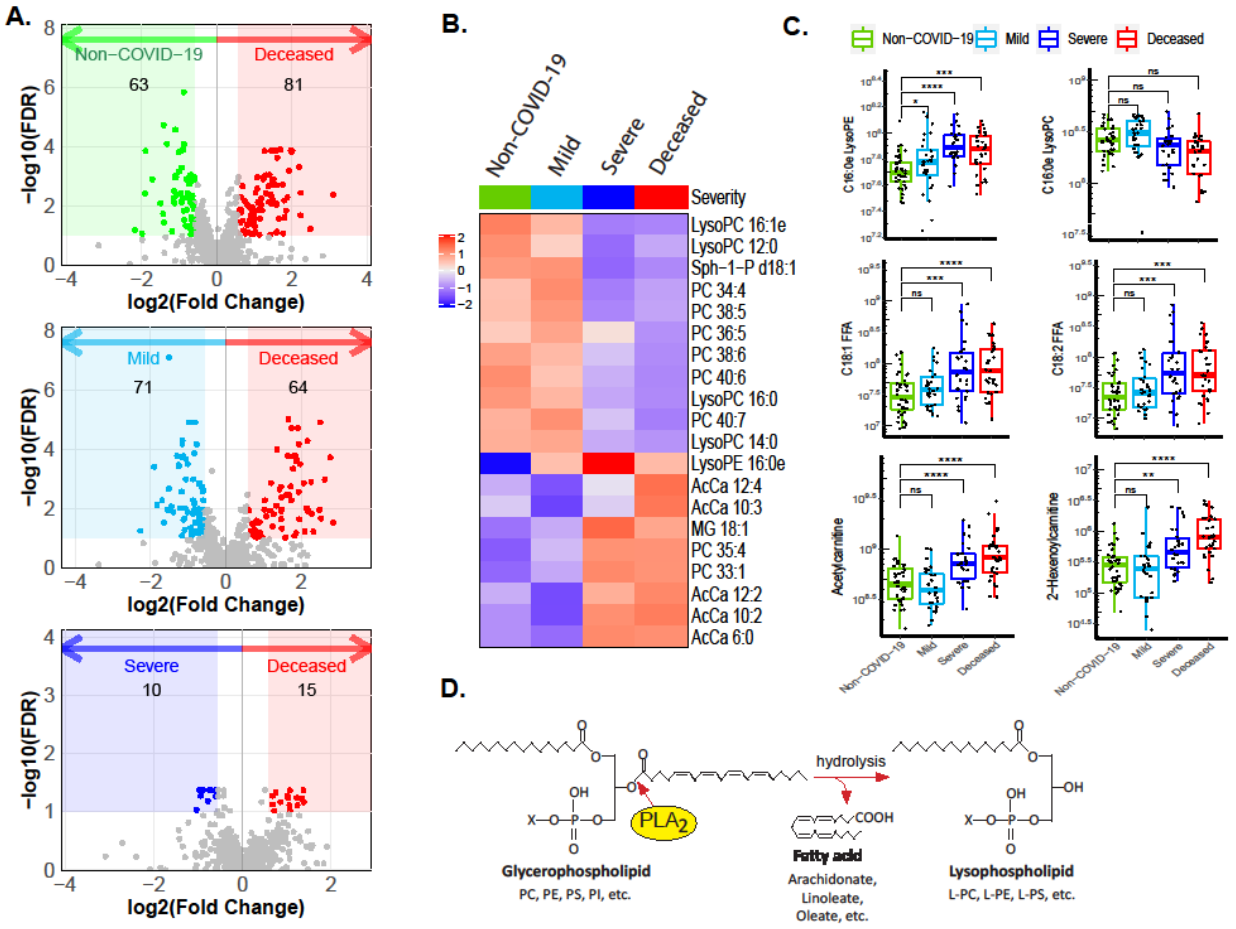

Figure 1. Untargeted lipidomic analysis and COVID-19 status. Plasma samples from non-COVID-19, mild, severe, and deceased COVID-19 patients were subjected to untargeted metabolomics analyses. Lipidome data were extracted from the metabolomics data set and analyzed. A) Volcano plots show significant alterations in the lipidome of the deceased COVID-19 patients compared with non-COVID-19, mild and severe COVID-19 patients. Colored areas highlight compounds with fold change (FC) greater than 1.5 and false discovery rate (FDR) less than 0.1. B) Heatmap of the top 20 metabolites whose abundances varied significantly across non-COVID-19, mild, severe, and deceased COVID-19 patients. C) Abundances of two lyso-phospholipids (lyso-PL), two free fatty acids (FFA) and two short chain acyl carnitines extracted from the untargeted lipid data. C16:0e LysoPC in the upper right is an example of a PC-containing lysolipid that did not meet the FC and FDR criteria in panel A and is not a primary substrate of $sPLA_2$-IIA. The other five compounds were selected from the colored regions in panel A (FDR<0.1) and may result from the action of $sPLA_2$-IIA. Levels in each panel were further compared using a one-sided Wilcoxon test with Holm correction for multiple testing. Box plot: the upper and lower bounds indicate the 75th (Q3) and 25th (Q1) percentile, respectively; the line within the box indicates the median value; whiskers extend to values within 1.5 IQR (the interquartile range, Q3 - Q1) of the upper or lower bound; outlying values are shown between 1.5 and 3 IQR beyond the upper or lower bound; the same below unless otherwise noted. Significance is indicated as: * p<0.05; ** p<0.01; *** p<0.001; **** p<0.0001. D) Model of PLA_2 reaction showing how PLA_2 hydrolyzes the sn-2 position of the glycerol backbone of phospholipids to form lyso-PL and FFA products.

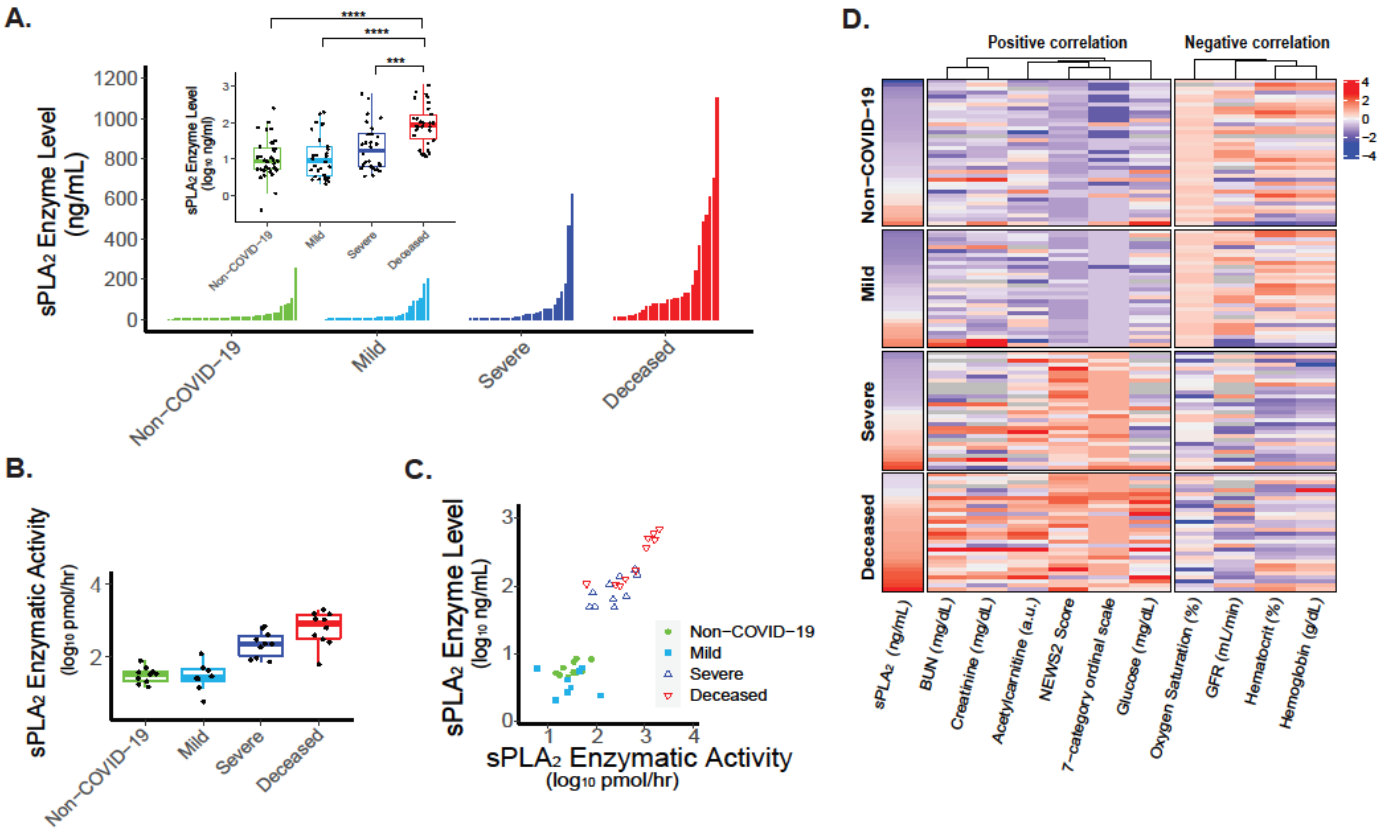

Figure 2. Association of sPLA$_2$-IIA and COVID-19 status. A) sPLA$_2$-IIA levels were determined in 127 plasma samples and are shown here sorted within each group. The inset boxplot compares the log-transformed data across groups and shows medians and quartiles. Groups were compared using a one-sided Wilcoxon test with Holm correction for multiple testing. Significance is indicated as: *** p<0.001; **** p<0.0001. Pairwise comparisons were computed from a linear model that included age and sex, and p-values were adjusted for multiple comparisons. B) sPLA$_2$ enzymatic activity within plasma was assayed in a selected subset of samples (see Supplementary Methods). C) The scatter plot shows plasma sPLA$_2$-IIA levels vs sPLA$_2$ activity in the selected subset of samples. Enzyme level and activity were strongly correlated, indicating plasma levels sPLA$_2$-IIA reflect levels of active enzyme in the larger sample set. D) A heatmap showing the significant Spearman correlations (FDR < 0.05) between sPLA$_2$-IIA and other clinical indices of disease severity. Indices that are positively or negatively correlated with sPLA$_2$-IIA are as indicated. Indices with missing values > 25 were removed, and those with skewness (absolute value) > 1.0 were log-transformed. Index values were mean-centered and scaled by the standard deviation. Blue to red represents low to high index values with color intensity indicating the value magnitude (see the color scheme). Missing values are shown in grey.

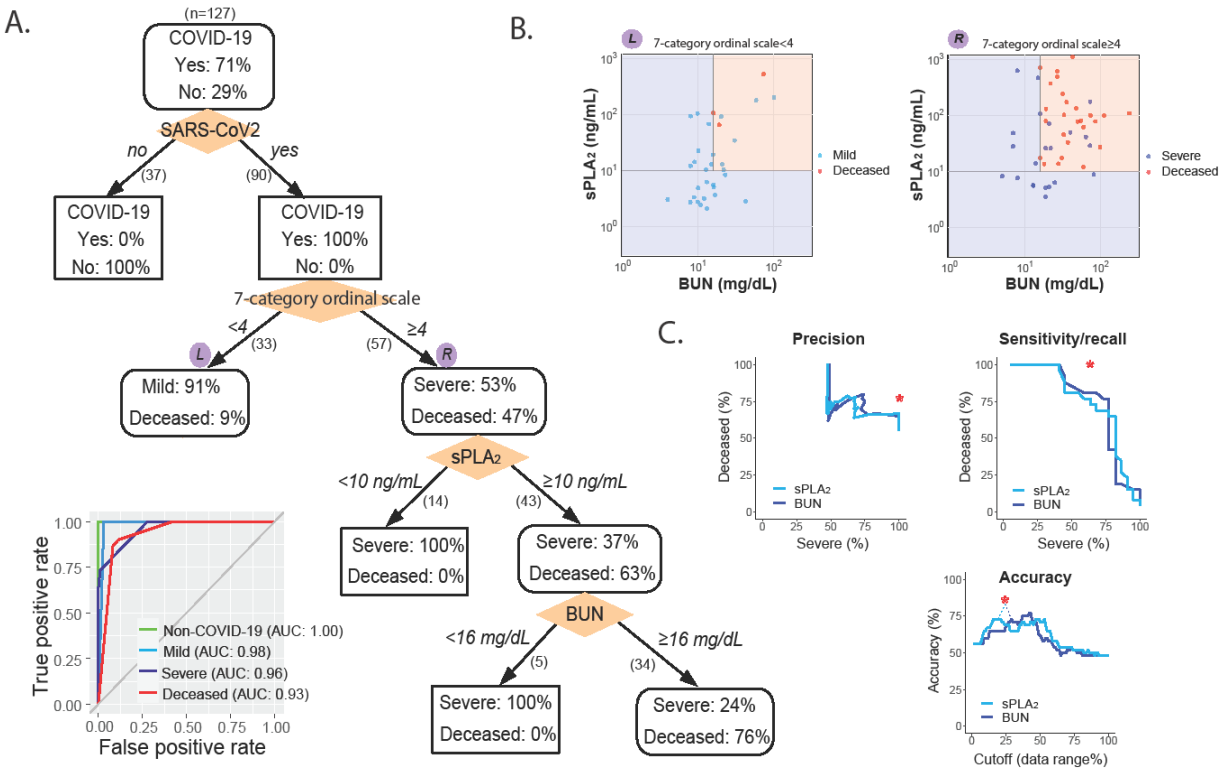

Figure 3. A Clinical decision tree predicting COVID-19 severity and mortality. A) The tree model. Patients are classified based on the indicated clinical indices (shown in orange diamonds) and boundary conditions (above split arrows). The number of patients following each split is shown in parentheses beneath the split arrow (patients with missing index values were not split). In each node, percentages of patients in corresponding categories are shown. (Inset) The area under the ROC curve, AUC, of the tree in determining each group membership (e.g., deceased vs. non-deceased). B) Decision surface based on the $sPLA_2$ and BUN boundary conditions in A. Left (L) and right (R) graphs show the results of applying the sPLA2 and BUN boundary conditions to the L and R subsets of patients (split following the 7-category ordinal scale), as indicated in A. C) The PLA-BUN index. The precision, sensitivity/recall, and accuracy in classifying severe and deceased COVID-19 patients (7-category ordinal scale $\geqslant$ 4) by combining both decision boundary conditions of sPLA2 and BUN as in B (i.e., the PLA-BUN index) are indicated with a red star in each graph, respectively. The corresponding classification results obtained by using the single index of sPLA2 (light blue curve) or BUN (dark blue curve) are shown with varying cutoff values in the corresponding data range (sPLA2, 3.4-1101.2 ng/mL; BUN, 5-242 mg/dL).

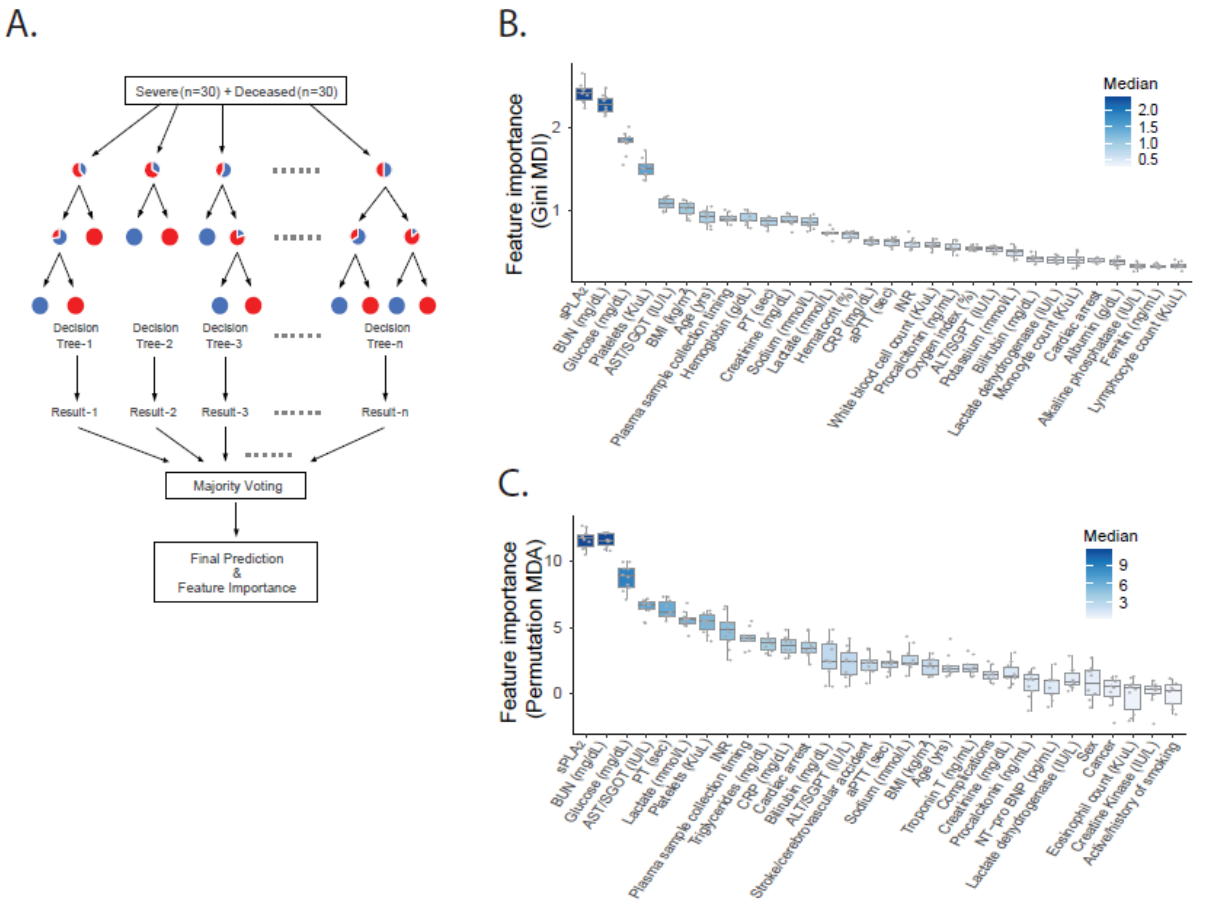

Figure 4. Feature importance ranking of clinical indices. The relative importance of the 80 clinical indices in separating the deceased from severe COVID-19 patients (n = 30 each) was evaluated in a random forest analysis (A). In this random forest, an assembly of decision trees (n = 1,000) were generated using randomly selected subsets of patients and features (clinical indices) to collectively arrive at the final model prediction (decreased vs. severe). The importance of a feature (i.e., clinical index) was evaluated by the decrease of prediction accuracy, when such a feature was excluded from the model, assessed based on the Gini impurity following a node split (B: MDI, Mean Decrease Impurity) and the permuted values of the feature (C: MDA, Mean Decrease Accuracy). The feature importance was evaluated in 10 repeated random forest analyses. The top 30 features in B and C are shown (color scheme is proportional to the importance score).

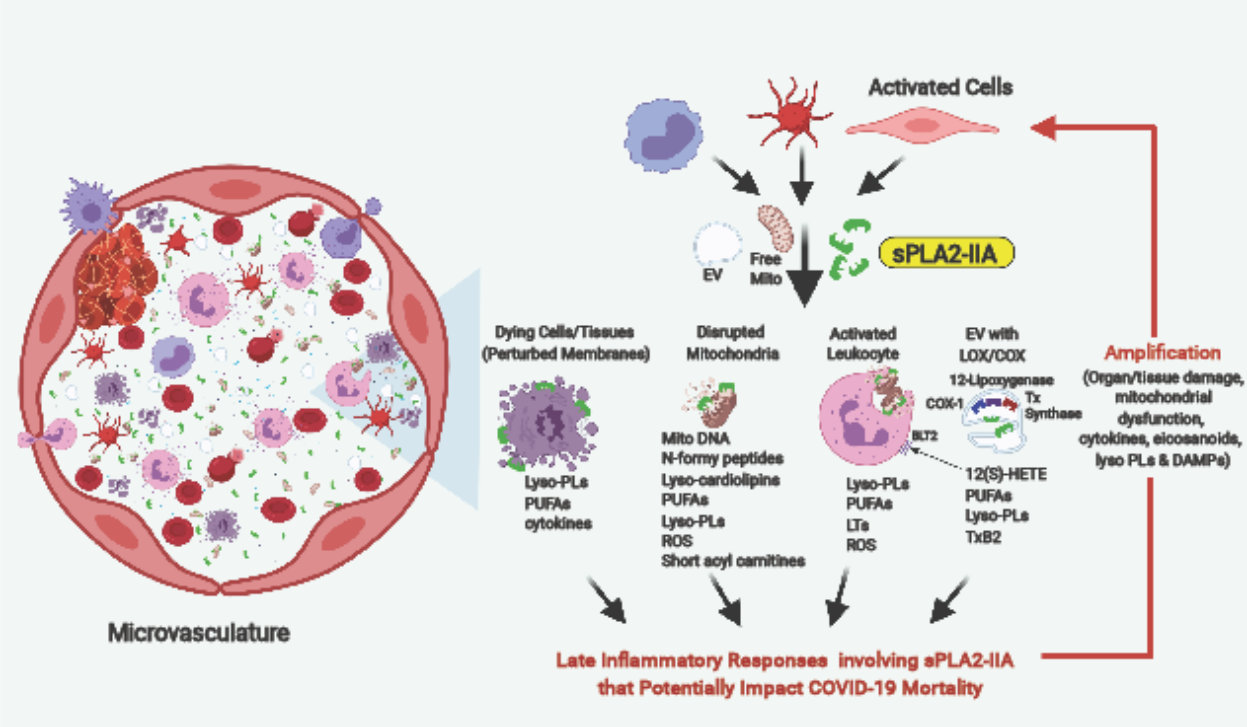

Figure 5. Potential direct and organism-wide pathogenic mechanism of sPLA$_2$-IIA. Mechanisms include: 1) hydrolysis of cellular membranes that broadly invoke tissue damage and organ dysfunction; 2) hydrolysis of mitochondrial membranes leading the release mtDNA, acetylcarnitine and DAMPs; 3) internalization of damaged mitochondria by bystander leukocytes to increase inflammatory mediators including lyso-PLs, unsaturated fatty acids, eicosanoids, and cytokines: and 4) hydrolysis of platelet-derived extracellular vesicles (EV) to release eicosanoids, platelet activating factor, and lyso-PLs.

TABLE 1: Demographics and Clinical Characteristics at Baseline

		COVID-19			
Variables	*Non COVID-19 (n=37)*	*Mild (n=30)*	*Severe (n=30)*	*Deceased (n=30)*	*p-value*
Demographics					
Mean age (range) – yr	57.08 (10-84)	53.37 (14-93)	62.4 (35-86)	71.17 (48-96)	0.0027
Sex: no. of patients (%)					
Male	20 (54.0)	12 (40.0)	16 (53.3)	20 (66.7)	0.2314
Female	17 (46.0)	18 (60.0)	14 (46.7)	10 (33.3)	
Race/ethnicity: no. of patients (%)					
White	28 (75.7)	19 (63.3)	14 (46.7)	19 (63.3)	0.0605
Black or African American	2 (5.4)	1 (3.3)	2 (6.7)	0 (0.0)	
Asian	1 (2.7)	0 (0.0)	0 (0.0)	4 (13.3)	
Hispanic or Latino	5 (13.5)	9 (30.0)	14 (46.7)	7 (23.3)	
Other	1 (2.7)	1 (3.3)	0 (0.0)	0 (0.0)	
Characteristics					
Median BMI, kg/m^2 (IQR)	29.54 (24.45-34.82)	28.55 (24.43-34.04)	29.3 (25.08-34.57)	25.86 (23.18-34.71)	0.0334
Median Charlson Comorbidity Index (IQR)	1 (0-2.5)	0 (0-2.25)	1 (0-3)	1 (0-3)	0.5738
Hypertension – no. of patients (%)	18 (48.7)	14 (46.7)	21 (70.0)	18 (60.0)	0.2167
Major cardiac disease[A] – no. of patients (%)	8 (21.6)	6 (20.0)	5 (16.7)	11 (36.7)	0.2687
Diabetes – no. of patients (%)	7 (18.9)	6 (20.0)	9 (30.0)	9 (30.0)	0.5856
Obesity[B] – no. of patients (%)	16 (43.2)	13 (43.3)	12 (40.0)	5 (16.7)	0.0859
Lipid disorder[C] – no. of patients (%)	13 (35.1)	9 (30.0)	12 (40.0)	10 (33.3)	0.8750
Kidney disease – no. of patients (%)	5 (13.5)	3 (10.0)	7 (23.3)	6 (20.0)	0.4865

Liver disease – no. of patients (%)	2 (5.4)	3 (10.0)	1 (3.3)	1 (3.3)	0.6352
Malignancy – no. of patients (%)	7 (18.9)	2 (6.7)	2 (6.7)	5 (16.7)	0.2945
Rheumatologic/connective tissue disease – no. of patients (%)	8 (21.6)	0 (0.0)	2 (6.7)	2 (6.7)	0.0179
Chronic lung disease, not asthma – no. of patients (%)	2 (5.4)	2 (6.7)	4 (13.3)	6 (20.0)	0.2215
Smoking – no. of patients (%)	17 (45.9)	8 (26.7)	8 (26.7)	8 (26.7)	0.2161
Asthma – no. of patients (%)	3 (8.1)	1 (3.3)	4 (13.3)	2 (6.7)	0.5422
[A]Major cardiac disease: coronary artery disease, congestive heart failure, history of myocardial infarction [B]Obesity defined as BMI $\geqslant$ 30 kg/m^2 [C]Lipid disorder: hyperlipidemia, dyslipidemia, antiphospholipid syndrome					

Demographics and clinical characteristics at baseline. All categorical variables are represented as proportions (%) whereas continuous variables are reported as median (interquartile range). D'Agostino-Pearson normality test was used to assess continuous variables and determined all that had non-Gaussian distributions; Kruskal-Wallis test was then used to assess for equality of group variance. Categorical variables were compared using the chi-square test. P-values reflect comparisons of group variance; significant trends are reported in Figure S1.